Earth and Planetary Science Letters 373 (2013) 129–139

Contents lists available at SciVerse ScienceDirect

Earth and Planetary Science Letters

journal homepage: www.elsevier.com/locate/epsl

Biogeochemical effects of atmospheric oxygen concentration, phosphorus weathering, and sea-level stand on oceanic redox chemistry: Implications for greenhouse climates

Kazumi Ozaki [a,*], Eiichi Tajika [b]

[a] Center for Earth Surface System Dynamics, Atmosphere and Ocean Research Institute, University of Tokyo, 5-1-5, Kashiwanoha, Kashiwa, Chiba 277-8561, Japan
[b] Department of Complexity Science and Engineering, Graduate School of Frontier Sciences, University of Tokyo, 5-1-5, Kashiwanoha, Kashiwa, Chiba 277-8561, Japan

ARTICLE INFO

Article history:
Received 25 July 2012
Received in revised form
19 April 2013
Accepted 20 April 2013
Editor: J. Lynch-Stieglitz
Available online 17 May 2013

Keywords:
anoxia
euxinia
biogeochemical cycles
atmospheric oxygen
continental shelf

ABSTRACT

Understanding the key factors influencing the global oceanic redox system is crucial to fully explaining the variations in oceanic chemical dynamics that have occurred throughout the Earth's history. In order to elucidate the mechanisms behind these variations on geological timescales, numerical sensitivity experiments were conducted with respect to the partial pressure of atmospheric molecular oxygen (pO_2), the continental shelf area (A_{cs}), and the riverine input rate of reactive phosphorus to the oceans (R_P). The sensitivity experiment for atmospheric pO_2 indicates that pervasive oceanic anoxia and euxinia appear when $pO_2 < 0.145$ atm and < 0.125 atm, respectively. These critical values of pO_2 are higher than a previous estimate of ~50% PAL (present atmospheric level) due to redox-dependent phosphorus cycling. The sensitivity experiment regarding the shelf area demonstrates that changes in the shelf area during the Phanerozoic significantly affected oceanic oxygenation states by changing marine biogeochemical cycling; a large continental shelf acts as an efficient buffer against oceanic eutrophication and prevents the appearance of ocean anoxia/euxinia. We also found that an enhanced R_P is an important mechanism for generation of widespread anoxia/euxinia via expansion of both the oxygen minimum zone and coastal deoxygenation, although the critical R_P value depends significantly on pO_2, A_{cs}, and the redox-dependent burial efficiency of phosphorus at the sediment–water interface. Our systematic examination of the oceanic redox state under Cretaceous greenhouse climatic conditions also supports the above results.

© 2013 Elsevier B.V. All rights reserved.

1. Introduction

The atmosphere–ocean system has remained in a fully oxygenated condition since at least the Devonian (e.g., Dahl et al., 2010; Strauss, 2006) with the exception of oceanic anoxic events (OAEs) (e.g., Jenkyns, 2010; Leckie et al., 2002). The oceanic oxygen inventory and distribution are controlled both by physical and biogeochemical processes. Therefore, previous studies conducted to elucidate the conditions and causal mechanism(s) of OAEs have mainly focused on two distinct mechanisms, namely, stagnation of ocean circulation and/or enhanced biological productivity in surface water (Handoh and Lenton, 2003; Hotinski et al., 2000, 2001; Meyer et al., 2008; Monteiro et al., 2012; Nederbragt et al., 2004; Ozaki et al., 2011; Sarmiento et al., 1988; Shaffer, 1989, 1996; Slomp and Van Cappellen, 2007; Southam et al., 1982, 1987; Tsandev and Slomp, 2009; Van Cappellen and Ingall, 1996; Winguth and Winguth, 2012). Ozaki et al. (2011) conducted systematic sensitivity experiments with respect to the intensity of the thermohaline circulation and riverine reactive phosphorus (P_{react}) input rate with HILDA-type (Joos et al., 1991; Shaffer and Sarmiento, 1995; Siegenthaler and Joos, 1992) biogeochemical ocean modeling. Together with an experiment concerning sea surface temperature (SST), they found the following results: (1) ocean stagnation causes deepwater anoxia, but widespread sulfidic (i.e., H_2S-rich) waters do not form by themselves; (2) a large SST increase (> 10 K) is required for the appearance of ocean anoxia, but euxinia cannot be caused even when the deviation of the SST from the reference value is greater than +15 K; and (3) riverine P_{react} input rate (R_P) of $> 1.4 \times R_P^*$ (asterisk represents the reference value; Table 1) causes ocean anoxia via expansion of the oxygen minimum zone (OMZ), and a value of $2.2 \times R_P^*$ results in global euxinia via enhancement of phosphorus (P) liberation from the sediment–water interface at the continental slope and shelves. An increase in R_P causes shelf anoxia, giving rise to

* Corresponding author. Tel.: +81 4 7136 6411.
E-mail address: ozaki@aori.u-tokyo.ac.jp (K. Ozaki).

0012-821X/$ - see front matter © 2013 Elsevier B.V. All rights reserved.
http://dx.doi.org/10.1016/j.epsl.2013.04.029

Table 1
Default parameter values.

Parameter		Unit	Reference value
Ocean circulation rate	$\dot{V}$	Sv (10^6 m^3/s)	20
Riverine P_{react} input rate	R_P	T mol P/yr (10^{12} mol P/yr)	0.18
Atmospheric pO_2	pO_2	atm	0.209
Shelf area	A_{cs}	10^{14} m^2	0.271
Sea surface temperature at L	SST^l	K	288.15
Sea surface temperature at H	SST^h	K	273.15

massive P liberation from sediments to bottom waters and, therefore, to global-scale anoxia (Ozaki et al., 2011; Tsandev and Slomp, 2009).

According to geologic evidence, OAEs tend to occur in warm climatic conditions and no OAE has been identified during "icehouse" climatic conditions, such as during the late Paleozoic and Cenozoic (Frakes et al., 1992; Jenkyns, 2010). However, the spatio-temporal extent of ocean anoxia is restricted, even during "greenhouse" climatic conditions. For Cretaceous OAEs, it is noteworthy that global-scale anoxia is not a persistent phenomenon and it generally lasts for less than a million years (e.g., Leckie et al., 2002; Sageman et al., 2006; Voigt et al., 2008). Hence, one can expect that a warm climate would be one of the necessary conditions for the occurrence of OAEs, although it would not be sufficient alone to cause them, implying the existence of additional causal factor(s). Recently, several studies have suggested that there is an intimate connection between Cretaceous ocean anoxia and the activities of large igneous provinces (LIPs) (Adams et al., 2010; Kuroda et al., 2007; Snow et al., 2005; Tejada et al., 2009; Turgeon and Creaser, 2008). Massive injections of greenhouse gases associated with the activity of LIPs might have caused a rapid warming of the climate (e.g., Ando et al., 2008; Forster et al., 2007), enhancement of chemical weathering on land (Blättler et al., 2011; Frijia and Parente, 2008; Tejada et al., 2009), and oceanic eutrophication/de-oxygenation (e.g., Kuypers et al., 2002; Mort et al., 2007a). However, the critical value of R_P, R_P^{crit}, as well as the required environmental perturbation of LIPs for the initiation of an OAE would be affected by other environmental factors, such as the background atmospheric oxygen concentration level. Without a quantitative understanding with respect to oceanic redox and its controlling factors, we cannot elucidate the ultimate causes of OAEs.

To clarify the relationship between long-term oceanic redox state and its controlling mechanisms, several factors must be considered, such as the atmospheric oxygen concentration (pO_2), sea-level stand (or shelf area; A_{cs}), nutrient loading flux from the continent to the ocean (R_P), ocean overturning rate, settling velocity of biogenic materials in the water column, and the sedimentation rate (SR), all of which have varied considerably over the Phanerozoic and which would affect the oxygen budget and distribution in the ocean due to changes in marine biogeochemical cycles. Among these, the atmospheric pO_2 level, A_{cs}, and R_P could have played fundamental roles in the oceanic redox state through direct or indirect causal mechanisms over the Phanerozoic eon.

The atmospheric pO_2 has a major and direct influence on the oxygen concentration in surface water, as well as in deepwater through the downwelling of surface waters in high latitude areas. It should therefore play a fundamental role in the long-term oceanic redox states. Previous evaluations with a three-box ocean model indicated that pervasive anoxia appears at $pO_2 < 50\%$ PAL (present atmospheric level), assuming the present availability of nutrients (e.g., Canfield, 1998; Lasaga and Ohmoto, 2002). This quantitative estimate of the critical pO_2 can be regarded as a lower estimate, because the phosphorus retention potential of marine sediment is depressed under the reducing conditions in the bottom water, giving rise to high phosphate availability in the anoxic ocean environment (e.g., Colman and Holland, 2000; Ingall and Jahnke, 1994; Van Cappellen and Ingall, 1996).

Sea level and coastal shelf area have varied considerably during the Phanerozoic (e.g., Miller et al., 2005; Müller et al., 2008; Ronov, 1994; Walker et al., 2002). High sea-level conditions are, in general, accompanied by greenhouse climatic conditions (e.g., early-middle Paleozoic and mid-Cretaceous). A shallow shelf is a primary locus for the deposition of biogenic materials because of a high rain flux of materials and high sediment accumulation rate (Berner, 1982; Dunne et al., 2007; Hedges and Keil, 1995). It can, therefore, be expected that a change in shelf area would have a critical role in the oceanic redox via changes in marine biogeochemical dynamics. Bjerrum et al. (2006) investigated the effect of sea-level change on oceanic biogeochemistry with a three-box ocean model coupled with an early diagenetic model of C, N, and P in seafloor sediments (Wallmann, 2003). The results indicated that a large expansion in shelf area would reduce the oxygen demand in the ocean, resulting in oxygenation of the open ocean. However, the overall effects of shelf size and other controlling factors (e.g., pO_2 and R_P) on the oceanic redox state have not been considered.

In this study, we set a three-step approach. First of all, we assess the long-term biogeochemical effect of pO_2 and A_{cs} on the oceanic redox condition. This makes clear how each factor affects the oceanic redox state as a result of changes in marine biogeochemical cycles. Next, we focus on how R_P^{crit} for the generation of oceanic anoxia/euxinia is affected by pO_2 and A_{cs} in order to gain insight into the long-term evolution of the marine redox state. Finally, the implications of this for the oceanic redox state under greenhouse climatic condition and causal mechanism of OAEs is discussed.

2. Methods

2.1. Model description

In order to shed light on the controlling factors of the long-term oceanic redox condition and the mechanism(s) behind the initiation of OAEs, we use a numerical model of the marine biogeochemical cycle. We employ an oceanic advection–diffusion–reaction biogeochemical cycle model (named *CANOPS*) to explore the impact of three causal factors (atmospheric pO_2; shelf area, A_{cs}; and riverine P_{react} input rate, R_P) on the oceanic redox state. CANOPS is an improved version of the transport-reaction model developed by Ozaki et al. (2011), which includes both physical and biogeochemical processes. The basic structure of CANOPS is illustrated in Fig. 1a. Below the surface water layers (L and H), the ocean interior comprises two regions: the high-mid latitude region ("young" deepwater region; YD) and low-mid latitude region ("old" deepwater region; OD). Each region is divided into 60 depth levels with a 100-m vertical grid spacing. The layers are labeled ($j=1,\ldots,60$) from the surface downwards. The total dissolved inorganic carbon (DIC), total alkalinity (ALK), oxygen (O_2), phosphate (PO_4^{3-}), nitrate (NO_3^-), ammonium (NH_4^+), sulfate (SO_4^{2-}), and total sulfide ($\sum H_2S$) are considered as dissolved chemical components of seawater. A further description of this model is presented in the Supplementary material.

2.2. Experimental setup

2.2.1. Atmospheric oxygen level

While several attempts have been made over the past three decades to reconstruct the variations in pO_2 during the Phanerozoic eon, the results vary widely (Bergman et al., 2004; Berner,

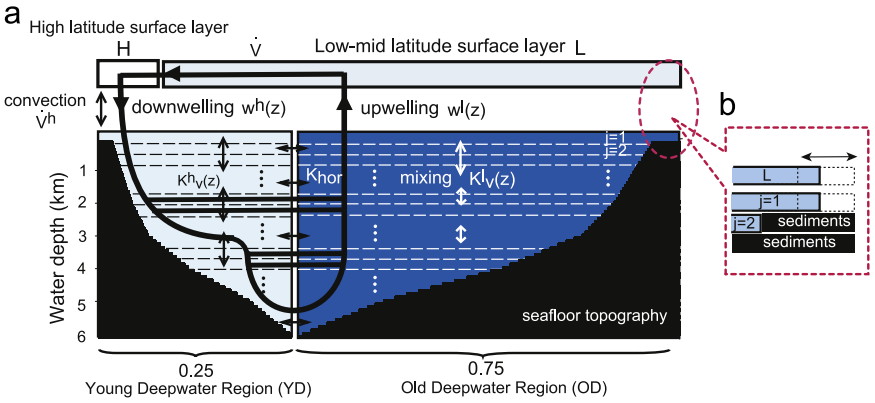

Fig. 1. (a) Schematic illustration of the model ocean used in this study. "L" and "H" denote the low-mid latitude mixed surface layer and high-latitude surface layer, respectively. An ocean area of 5% is assumed for the high-latitude surface box. The area of the young deepwater sector (YD) is 25% of the whole ocean. $K_v^l(z)$ and $K_v^h(z)$ are the vertical eddy diffusion coefficients in the OD and YD regions, respectively, and K_{hor} and $\dot{V}^h$ are the horizontal diffusion coefficient and polar convection, respectively. The seafloor topography assumed in this study is depicted as black hatch. (b) Schematic concept for modeling the shelf area change.

1989, 2009; Falkowski et al., 2005; Glasspool and Scott, 2010; Lasaga, 1989). The variations of the oceanic redox state over this interval have been reviewed by several researchers (Dahl et al., 2010; Meyer and Kump, 2008; Strauss, 2006). However, the evolution of the oceanic redox state and its quantitative relationship with the atmospheric redox state are not yet clear.

In order to assess the influence of the atmospheric pO_2 level on the global oceanic redox state, we assume that the surface water is in equilibrium with the atmosphere, and that the equilibrium oxygen concentration scales linearly with the atmospheric oxygen concentration:

$$[O_2]^{l,h} = [O_2](SST^{l,h}, SSS^{l,h})\frac{pO_2}{pO_2^*} \quad (1)$$

where the saturated concentration is calculated from the solubility of oxygen in seawater at a given SST, sea surface salinity (SSS) (35 psu for L and 34 psu for H) (Garcia and Gordon, 1992), and atmospheric oxygen partial pressure. Here, l, h, and ∗ represent the low-mid-latitude region, high-latitude region, and reference values (Table 1), respectively.

Given the residence time of O_2 in the atmosphere–ocean system (2–4 million years; Catling and Claire, 2005; Lenton, 2003; Walker, 1974), pO_2 changes relatively slowly in comparison to ocean phosphorus cycling (timescale of 10,000 yr) and ocean redox state (timescale of several thousands of years). Because we focus mainly on the secular effect of pO_2 on marine biogeochemistry and requisite conditions for OAE, the atmospheric pO_2 can be treated as a boundary condition in this study.

2.2.2. Shelf area

In order to represent the change in A_{cs} in the model, we change the areas of the surface and $j=1$ layers, as shown in Fig. 1b. A_{cs}^* is about 0.27×10^{14} m^2, occupying ~7.5% of whole ocean area today. The burial efficiency of C_{org} on shelves is generally high (approximately 40–80%; Betts and Holland, 1991; Henrichs and Reeburgh, 1987). Hence, as the shelf area increases, the ratio of the C_{org} burial flux to export flux for the whole ocean increases (1.37% and 2.3% for shelf areas of 100% and 200% of the present value, respectively).

Variations in sea level and shelf area during the Phanerozoic have been studied geologically and geomorphologically. According to comprehensive studies conducted by Alexander Ronov and his colleagues, the shelf area was tectonically controlled and exhibited two maximums during the Paleozoic and Cretaceous (e.g., Ronov, 1968, 1994). More recent estimates, which show that the shelf area at low-mid latitudes was 2–3 times larger during the Paleozoic and Cretaceous than at present, do not change this conclusion (Walker et al., 2002).

2.3. Redox index and edge of anoxia/euxinia

We categorize the oceanic redox state into six types based on the distributions of dissolved oxygen (OXIA=oxic ocean, IWA=intermediate water anoxia, and DWA=deep water anoxia) and hydrogen sulfide (non-sulfidic, IWE=intermediate water euxinia, and DWE=deep water euxinia) in the ocean interior (Ozaki et al., 2011). This categorization provides information on the redox state of the ocean and may allow us to consider the causal mechanisms. It does not, however, provide any quantitative information on the spatial extent of anoxia/euxinia. In order to represent the spatial extent of reducing environments in the ocean, we introduce the "redox index" (RI), which is defined as follows:

$$RI^{l,h} \equiv \frac{\int i^{l,h}A^{l,h}dz}{\int A^{l,h}dz} = \frac{1}{V^{l,h}}\int_{-z_b}^{-h_m} i^{l,h}A^{l,h}dz \quad (2)$$

where V^l and V^h are the oceanic volume of the OD and YD regions, A is the areal fraction of the water layer at depth z to the global sea surface area, and i is an index at each water depth, defined as follows:

$$i = \begin{cases} 0.0 & \text{for oxic water } ([O_2] > 0.001 \text{ mol/m}^3) \\ 0.5 & \text{for anoxic, non}-\text{sulfidic water } ([O_2] < 0.001 \text{ mol/m}^3 \text{ and } [\sum H_2S] < 0.1 \text{ mol/m}^3) \\ 1.0 & \text{for euxinia } ([\sum H_2S] > 0.1 \text{ mol/m}^3) \end{cases} \quad (3)$$

We also define a globally averaged redox index as follows:

$$\overline{RI} \equiv \frac{\int i^l A^l dz + \int i^h A^h dz}{V^l + V^h}. \quad (4)$$

The redox index is close to 0.5 as anoxia extends to within the ocean interior, and is close to unity as pervasive euxinia appears.

We also introduce the "Edge of Anoxia/Euxinia" as follows:

$$\begin{cases} \text{Edge of Anoxia}: & 0.0 < RI^l \le 0.4 \\ \text{Edge of Euxinia}: & 0.5 < RI^l \le 0.9 \end{cases} \quad (5)$$

The Edge of Anoxia (EoA) approximately corresponds to the transition of the oceanic redox state between an oxygenated condition and an anoxic condition, and the Edge of Euxinia (EoE) is an indicator of the spatial extent of sulfidic waters in the ocean interior.

3. Results

3.1. Effect of atmospheric pO_2

The response of the oceanic biogeochemistry to changes in pO_2 is illustrated in Fig. 2. In these calculations, we assumed reference values for the other controlling factors (Table 1). As expected, O_2 concentrations decrease with decreased pO_2 and vice versa (Fig. 2c). In the OD region, anoxia (defined as $[O_2] < 0.001$ mol/m^3) appears when pO_2 is below 0.175 atm. The DWA appears at $pO_2 < 0.145$ atm, and a transition to pervasive euxinia (defined as the concentration of total sulfide $[\Sigma H_2S] > 0.1$ mol/m^3) occurs around pO_2 values below 0.125 atm. EoA and EoE appear for $pO_2 = 0.145$–0.175 atm and $pO_2 = 0.115$–0.125 atm, respectively (Fig. 2a). In the YD region, anoxia and euxinia appear when pO_2 is below 0.135 atm and 0.100 atm, respectively. The formation of deepwaters in high-latitude regions supplies "fresh" (i.e., cold, oxygen-rich) waters to YD regions, thus preventing the generation of oceanic anoxia relative to the OD region.

It is noteworthy that the decline of the oceanic oxygen concentrations results not only from the direct effect of atmospheric pO_2 on the oxygen concentration in the surface water, but also from the behavior of marine P cycling. The decrease in surface O_2 promotes de-oxygenation in the surface ocean, yielding an expansion of the OMZ (Fig. 2c). Preferential regeneration of phosphorus from organic matter in the seafloor sediment in the OMZ (Van Cappellen and Ingall, 1996), represented as an increase in C_{org}/P_{react} value of buried sediment in Fig. 2b, enhances phosphate concentration in the ocean (Fig. 2d), leading to an increase in surface productivity (Fig. 2b). This biogeochemical behavior (anoxia-productivity feedback; e.g., Algeo and Ingall, 2007) gives rise to further expansion of the OMZ. In particular, biological production is markedly enhanced at the EoE. This corresponds to a pronounced increase in the C_{org}/P_{react} ratio. Under such circumstances, anoxic waters reach the shelf region. This leads to a massive P release from shelf sediments to bottom waters, dragging the ocean into a pervasive euxinic condition. Further increases in C_{org} export production and the C_{org}/P_{react} ratio of buried sediments at $pO_2 < 0.115$ atm mainly reflect the expansion of anoxia in the YD region. At a pO_2 of 0.05 atm, the oceanic interior is widely deoxygenated, and the C_{org}/P_{react} ratio approaches its maximum value of ~200 (Fig. 2b). In that case, the global export production of C_{org} increases to more than three times the reference value owing to the efficient recycling of P in the ocean interior. It is noteworthy that this ~200 upper limit to the C_{org}/P_{react} ratio is deduced from observations of modern permanently anoxic environments, such as the Black Sea, the inner basin of Effingham Inlet, and the Framvaren Fjord (e.g., Algeo and Ingall, 2007). In contrast, evidence for decreases in phosphorus accumulation and increases in the C_{org}/P_{react} ratio up to 1500 during Cretaceous OAE2 has been reported (Kraal et al., 2010; Mort et al., 2007a; Nederbragt et al., 2004). Therefore, the intensity of anoxia-productivity feedback assumed in this study can be regarded as an underestimation.

In the oxygen-depleted oceans, enhanced denitrification tends to reduce marine fixed nitrogen (nitrate and ammonium). Nitrogen depletion is assumed to be compensated by fixation of nitrogen from the atmosphere in this model (Supplementary material). Therefore, nitrogen fixation required for maintaining the biological productivity should be enhanced. For instance, nitrogen fixation rate required to the nitrogen balance would be ~2580 Tg N/yr when $pO_2 = 0.1$ atm (not shown). This value is ~22 times the reference (preindustrial) value of 118 Tg N/yr. If the activity of nitrogen fixation is limited for some reasons (e.g., exhaustion of trace metals, such as Mo), marine biological productivity cannot be increased because of the limiting of nitrogen.

3.2. Effect of shelf size

The effects of A_{cs} on the distributions of dissolved oxygen and phosphate in the ocean are shown in Fig. 3c and d, respectively. As the shelf area decreases, the ability of shallow sediments to retain P is diminished. This leads to increased dissolved P concentrations (Fig. 3d) and increased rates of primary production (Fig. 3b). In the OD region, anoxia appears at intermediate depths (at ~1000 m) when A_{cs} is less than approximately 70% of the

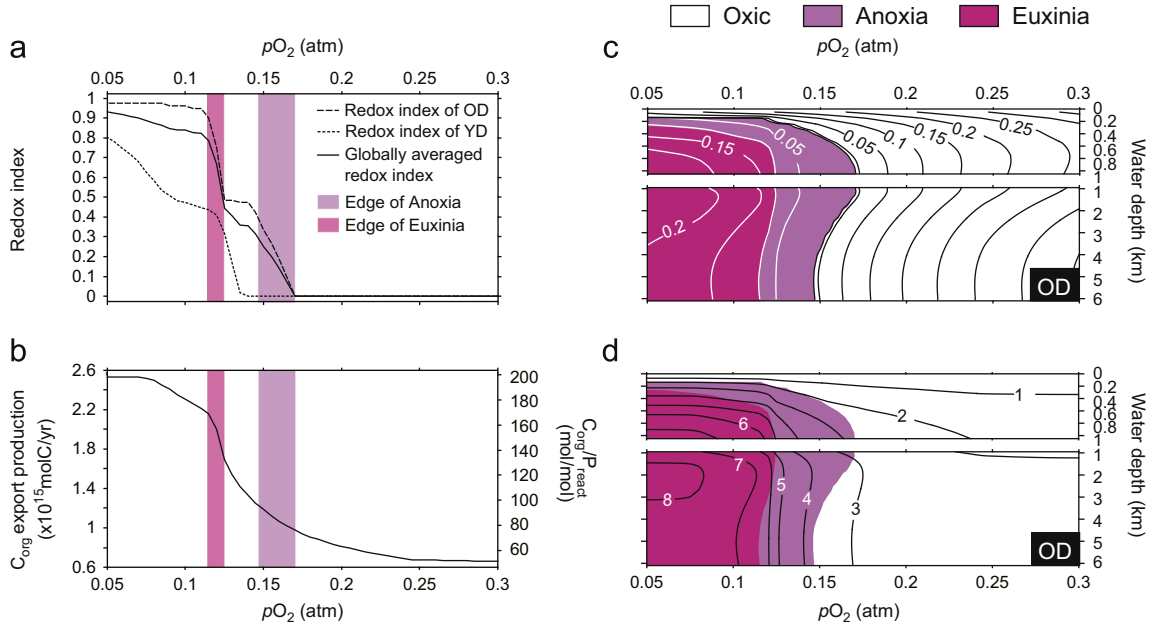

Fig. 2. Effect of atmospheric oxygen concentration on the ocean biogeochemistry. (a) Redox indexes. "Edge of Anoxia" and "Edge of Euxinia" for the OD region are represented by light and dark shading. (b) Export production of organic carbon (in 10^{15} mol C/yr) and globally averaged C_{org}/P_{react} ratio of buried sediments. (c) Oxygen (black lines) and ΣH_2S (white lines) distribution for OD region (in mol/m^3). (d) Phosphate distribution for OD region (in mmol/m^3). In (c) and (d), anoxia and euxinia are represented by light and dark shading, respectively.

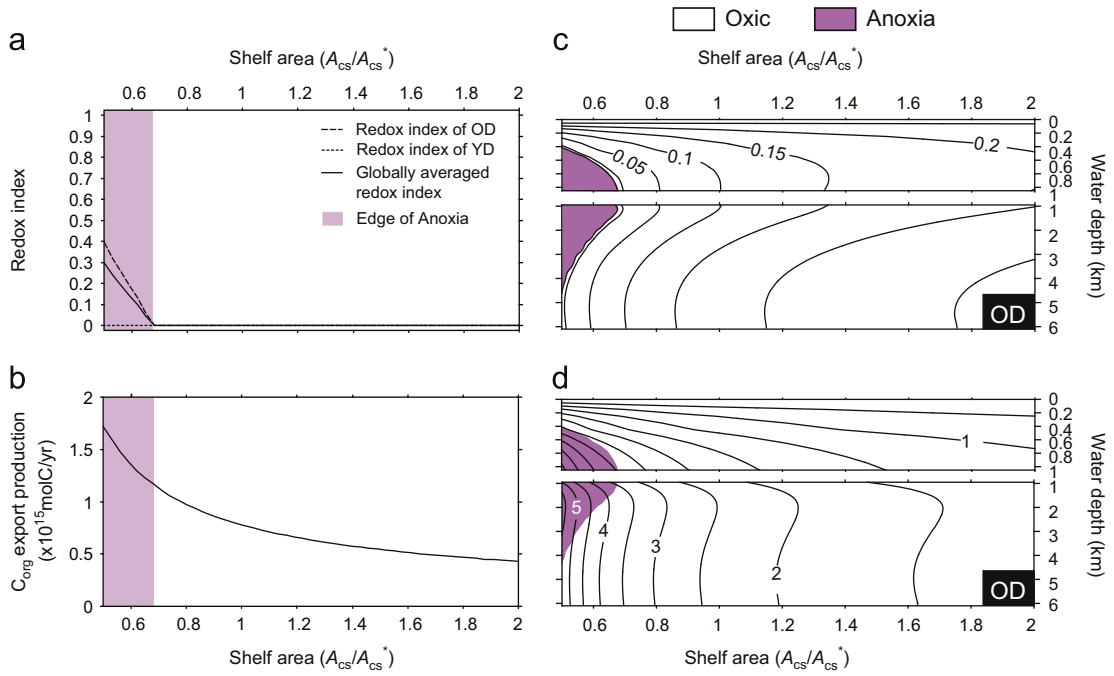

Fig. 3. Effect of shelf area on ocean biogeochemistry. (a) Redox indexes. "Edge of Anoxia" for the OD region is represented by light shading. (b) Export production of organic carbon (in 10^{15} mol C/yr). (c) Oxygen distribution for the OD region (in mol/m^3). (d) Phosphate distribution for the OD region (in mmol/m^3). In (c) and (d), anoxia is represented by light shading.

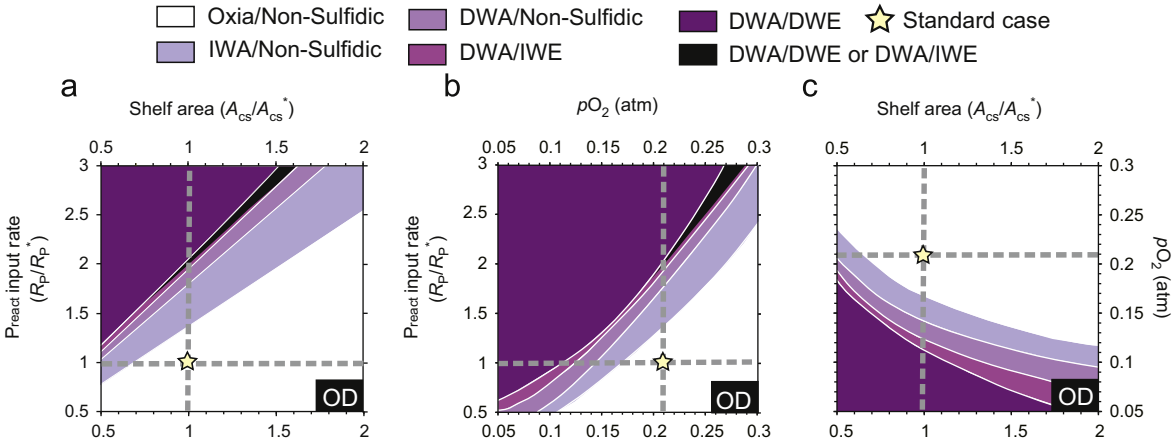

Fig. 4. Steady-state ocean redox state for the OD region; diagrams for (a) riverine P_{react} input rate from continent to ocean (R_P/R_P^*) and shelf area (A_{cs}/A_{cs}^*), (b) R_P/R_P^* and atmospheric pO_2, and (c) pO_2 and A_{cs}/A_{cs}^*, where the asterisk represents the reference condition (Table 1). Oceanic redox conditions based on oxygen and hydrogen sulfide profiles. OXIC, IWA, and DWA denote fully oxic conditions, intermediate water anoxia, and deepwater anoxia, respectively, and non-sulfidic, IWE, and DWE denote non-sulfidic conditions, intermediate water euxinia, and deepwater euxinia, respectively (Ozaki et al., 2011). In (a) and (b), the parameter region where bistable solutions (DWA/DWE or DWA/IEW) exist is colored by black shading.

reference value (Fig. 3a and c). When $A_{cs}=0.5\times A_{cs}^*$, anoxia appears at water depths of ~400–4000 m, occupying ~39% of the volume of OD region. However, euxinia does not occur in this experiment. By contrast, the vast shelf area should trap large amounts of nutrients, which include phosphorus, resulting in the ocean being in a more oligotrophic and oxygenated condition. For instance, doubling A_{cs} gives rise to a ~45% decline in C_{org} export production relative to the reference state (Fig. 3b). This behavior supports previous results obtained by Bjerrum et al. (2006), suggesting the possibility that the vast shelf area may act as an efficient buffer against oceanic eutrophication and generation of anoxia.

According to geographical studies (Ronov, 1994; Walker et al., 2002), shelf areas in low-mid latitude region were over 200% of present value during "greenhouse" climatic periods, such as the mid-Cretaceous. Our model demonstrates that ocean tended to be more oligotrophic and well oxygenated in those periods than at present if other parameters are assumed to be the same. Therefore, changes in sea level stands and shelf area throughout geological history could have a quantitative importance for discussions of the paleo-oceanic redox state.

3.3. Oceanic redox conditions with respect to pO_2, A_{cs}, and R_P

Next, we systematically examine steady-state oceanic redox conditions for three parameters (pO_2, A_{cs}, and R_P). Fig. 4a represents the oceanic redox conditions in a steady state with respect to R_P/R_P^* and A_{cs}/A_{cs}^* in the OD region. The reference condition is represented as an asterisk in this figure. The enhanced phosphorus input is clearly crucial for the generation of anoxia/euxinia in the ocean. However, it is noteworthy that the R_P^{crit} for the initiation of

anoxia/euxinia depends strongly on A_{cs}. For instance, $R_P > \sim 2.8 \times R_P^*$ is required when $A_{cs} = 1.5 \times A_{cs}^*$ for the generation of euxinia, although the threshold is approximately $2.0 \times R_P^*$ under the present value of A_{cs}. Fig. 4a indicates that vast shelf area would act as an efficient buffer of oceanic eutrophication and anoxia/euxinia.

Fig. 4b shows oceanic redox conditions with respect to R_P/R_P^* and pO_2 in the OD region, assuming the present value of A_{cs}. This diagram indicates that R_P^{crit} increases with pO_2; while the value of R_P^{crit} necessary to initiate anoxia and euxinia is $1.4 \times R_P^*$ and $2.0 \times R_P^*$ at a pO_2 of 0.21 atm; these numbers are only $0.8 \times R_P^*$ and $1.35 \times R_P^*$ at $pO_2 = 0.15$ atm. On the other hand, $R_P > \sim 2.5 \times R_P^*$ is required for anoxia to appear under $pO_2 = 0.30$ atm. This quasi-linear relationship can be explained by a simple balance of oxygen supply (via pO_2) and demand (via R_P). Considering a pO_2 range of ~0.15–0.35 atm estimated from mass balance models (e.g., Berner, 2009) during the Phanerozoic, changes in pO_2 play a fundamental role in discussions of not only the long-term evolution of paleoredox but also of the conditions necessary for the occurrence of OAEs.

In Fig. 4a and b, we found bistable solutions for the oceanic redox condition (colored by black shading). For instance, under the conditions of $R_P = 2 \times R_P^*$, $A_{cs} = A_{cs}^*$, and $pO_2 = pO_2^*$, there are two stable redox structures, DWA/IWE and DWA/DWE, depending on the initial condition. This bifurcation originates from the strong non-linearity of the redox-dependent marine P cycling. In particular, once shelf anoxia (anoxia at $j=1$ layer) is achieved, an enhanced recycling of P sustains the DWA/DWE condition.

The redox conditions with respect to pO_2 and A_{cs}/A_{cs}^* with a reference value of R_P (Fig. 4c) show that the oceanic redox state is affected by pO_2 and A_{cs}. Considering the plausible variation ranges of A_{cs} (~ 0.5–$3.0 \times A_{cs}^*$) and pO_2 (~0.15–0.35 atm) during the Phanerozoic eon, this diagram demonstrates that the oceanic redox state will be basically oxic as long as the present value of R_P is assumed (except for assuming the conditions of very low pO_2 and much smaller A_{cs}). In summary, an enhanced P_{react} input rate is fundamental for the initiation of OAEs, and the required P_{react} input rate depends on the values of A_{cs} and pO_2.

4. Discussion

4.1. Implications for the relationship between pO_2 and marine redox chemistry

The long-term oceanic redox history has previously been discussed based on the evolution of the atmospheric oxygenation state. Our sensitivity experiment with respect to the atmospheric pO_2 level (Fig. 2) provides some insights into the oceanic redox evolution through the Earth's history. Fig. 2c indicates that global anoxia (DWA) in the low–mid latitude region appeared at $pO_2 < 0.145$ atm. This pO_2 value is larger than the previously estimated value of ~0.1 atm based on a three-box model (Canfield, 1998; Lasaga and Ohmoto, 2002). This is largely because our model includes the process of redox-dependent phosphorus liberation at the sediment–water interface (Colman and Holland, 2000; Ingall and Jahnke, 1994). Therefore, once anoxia appears in the water column, preferential regeneration of P relative to C enhances oceanic surface productivity (Fig. 2b), resulting in more reducing conditions. Without this mechanism, global anoxia occurs at $pO_2 < 0.09$ atm (Fig. 5), which is consistent with previous estimates (Canfield, 1998). Therefore, redox-dependent P cycling exerts a crucial role in the conditions for a generation of anoxia/euxinia.

The obtained threshold of pO_2 between pervasive anoxia and euxinia is $pO_2 \sim 60\%$ PAL, and a fully oxic condition is not achieved until pO_2 is above 0.175 atm (Fig. 2). Recent combustion experiments

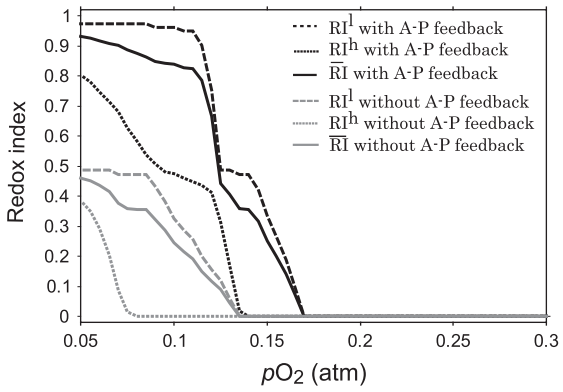

Fig. 5. Effect of atmospheric oxygen concentration on the redox index with (black lines) and without (gray lines) "anoxia-productivity feedback." Redox indexes for OD and YD are represented as dashed and dotted lines. The global mean redox index is depicted as a solid line.

(Belcher et al., 2010) shows that fire activity would be greatly suppressed when $pO_2 < \sim 0.18$ atm. On the other hand, there is a continuous record of charcoal since the Devonian (e.g., Algeo and Ingall, 2007; Glasspool and Scott, 2010). Therefore, it seems likely that atmospheric pO_2 has been $> \sim 0.18$ atm since the Devonian. This value is roughly equal to the critical value for initiation of OAEs estimated from our study (Fig. 2). Recently, Dahl et al. (2010) presented the molybdenum isotopic value in sedimentary rocks and found a global oceanic oxygenation around the Silurian–Devonian period. If an increase in δ^{98}Mo up to 2.0‰ can be regarded as a global oceanic oxygenation, such an oxygenation event would reflect the condition of $pO_2 > 0.175$ atm. Here, we must note that the pO_2 threshold is also a function of several environmental factors, such as R_P and A_{cs} (Fig. 4b and c). If R_P is lower than that at present, the required pO_2 for oxygenation of the whole ocean also decreases, and vice versa. If R_P is 50% of the present value, then the threshold between oxic and anoxic oceans decreases to 0.105 atm, as shown in Fig. 4b.

The sensitivity experiment of pO_2 also provides insight into the Precambrian ocean redox state. The Proterozoic ocean was probably under anoxic (ferruginous/sulfidic) conditions, based on geological and geochemical data, such as sulfur isotopic composition (e.g., Canfield, 1998), iron speciation data (Canfield et al., 2008; Li et al., 2010; Planavsky et al., 2011; Poulton et al., 2010; Shen et al., 2002, 2003), and Mo concentrations (Scott et al., 2008). The reducing oceanic conditions are considered to be associated with low atmospheric pO_2 levels, but the actual value of atmospheric pO_2 during the Proterozoic are not well defined. Our model demonstrates that pervasive euxinia will occur at $pO_2 < 0.125$ atm (Fig. 2c). This transition of oceanic redox reflects the occurrence of shelf anoxia; anoxia at continental shelves effectively promotes a massive liberation of P from sediments to bottom waters, leading to marine eutrophication and generation of euxinia. Without considering the anoxia-productivity feedback (A–P feedback), pervasive euxinia cannot be achieved even when $pO_2 = 0.05$ atm (Fig. 5). This is because the quantity of organic matter available for sulfate reduction is not enough to accumulate H_2S in high concentrations.

We note that, in the past, the intensity of the biological pump was very different to that of the present ocean. In fact, the present biological pump is efficient, owing to large quantities of fecal pellets derived from zooplankton and high-density biominerals, such as opal (2.1 g/cm^3) and carbonate (2.71 g/cm^3), and sinking particulate organic matter (POM), and these biogenic materials act as a "shuttle" to the abyssal ocean. Because of this process, which is known as the "ballast effect" or "ballast hypothesis" (Armstrong et al., 2002; Ittekkot, 1993; Klaas and Archer, 2002), the delivery of

biogenic materials to deepwater may not have been efficient before diversification of coccolithophores, foraminifera, and/or diatoms. If the intensity of the biological pump is weaker than at present because of a lower sinking velocity and/or higher degradability, the oxygen demand in the surface-intermediate waters would have been larger than at present (Kashiyama et al., 2011; Logan et al., 1995), giving rise to a threshold between oxic and anoxic oceans with a value greater than 0.145 atm. This idea provides further speculation for the discussion on marine redox chemistry in the aftermath of mass extinction (e.g., Permian–Triassic boundary ~251 Ma); efficient recycling of POM in a shallow part of the ocean promotes shelf anoxia, resulting in further eutrophication and anoxia by stimulating A–P feedback.

In summary, the relationship between the atmospheric pO_2 and oceanic redox state is affected significantly by several factors, including R_P, A_{cs}, ballast effect, among others. Hence, we must carefully consider these settings to quantitatively constrain the redox evolution of atmosphere–ocean system.

4.2. Oceanic redox states under Cretaceous greenhouse climatic condition

Figs. 3 and 4a demonstrate that vast shelf area may act as an efficient buffer against oceanic eutrophication and generation of anoxia/euxinia. This biogeochemical behavior will be important for discussions of the oceanic redox condition in ancient "greenhouse" climates. For instance, in the mid-Cretaceous, which is known as a prominent "greenhouse world", the concentration of atmospheric carbon dioxide is estimated to have been ~1000 ppmv (Hong and Lee, 2012; Park and Royer, 2011; Royer et al., 2012), and the reconstructed seawater temperature shows higher values than those at present (e.g., Friedrich et al., 2012; Pucéat et al., 2003). During the Cretaceous it is likely that CO_2 degassing rate from solid earth into the atmosphere–ocean system was probably higher than at present (e.g., Larson, 1991). Under warm and wet climatic conditions, an enhanced hydrological cycle could accelerate chemical weathering on land, leading to an enhanced delivery of nutrients to the ocean. If it is the case then ocean would tend to be de-oxygenated owing to the combined effect of enhanced nutrient input and a decrease in O_2 solubility in surface waters (Ozaki et al., 2011).

On the other hand, according to paleogeographic reconstructions, the mid-Cretaceous was accompanied by high sea-level conditions and vast shelf area of ~177–220% of that at present (Bjerrum et al., 2006; Ronov, 1994; Walker et al., 2002). If other factors are kept constant, export productivity decreases by ~40–52% relative to present value and the oxygen inventory of the ocean increases (Fig. 3). Therefore, because the vast shelf area acts as a major sink of nutrients delivered from the continent, oxic environments may have occurred in such a greenhouse world (Figs. 3 and 4a).

To assess the oceanic redox state underlying the greenhouse climatic condition and to highlight the biogeochemical effect of shelf area under such conditions, we conducted a systematic sensitivity experiment with respect to pO_2 and A_{cs} under the Cretaceous conditions (Fig. 6a). In this calculation R_P is estimated using a simple weathering scheme which includes several controlling factors on the chemical weathering rate (see Appendix A). As a result, we estimate R_P to be $\sim 1.38 \times R_P^*$ for the Cretaceous. Based on temperature reconstructions from $\delta^{18}O$ values of carbonate (e.g., Royer et al., 2004), we assume that the SST increases by 4 K for L. Considering a small thermal equator-to-pole gradient (e.g., Bice and Norris, 2002) and high deepwater temperature (e.g., Friedrich et al., 2012), we assume an increase in SST of +10 K for H. Considering the low physical erosion rate during the Cretaceous (Berner and Kothavala, 2001), we also assumed a low sedimentation rate relative to the present value.

Fig. 6a demonstrates that the Cretaceous oceanic redox was significantly affected by A_{cs}. The ocean would have been in pervasive anoxia/euxinia (DWA/DWE) when $pO_2 = pO_2^*$ and $A_{cs} = A_{cs}^*$. This is the result of the combined effect of an enhanced R_P and decreased oxygen solubility. When $A_{cs} = A_{cs}^*$, the ocean cannot be oxygenated unless $pO_2 > \sim 0.31$ atm. On the other hand, given the geological constraints of the shelf area during the Cretaceous (~200% of present; Ronov, 1994; Walker et al., 2002), the ocean will be oxygenated when $pO_2 > \sim 0.21$ atm. The vast shelf area plays a crucial role in the Cretaceous oceanic redox state.

In general, vast A_{cs} (and high sea-level stand) conditions reflect an increased oceanic crust production rate (e.g., Müller et al., 2008). An active tectonic forcing such as enhanced CO_2 degassing gives rise to warm climatic condition via accumulation of CO_2 in the atmosphere on the timescales of $> 10^{5-6}$ yr. Under warm climatic conditions, chemical weathering on land would be enhanced, leading to an increase in nutrient discharge to the ocean. However, oceanic eutrophication could be buffered by the vast shelf area (Figs. 3 and 6a). Therefore, our results highlight the intimate connection between the tectonic conditions, sea-level stand, climate, and long-term oceanic redox state: increased CO_2 degassing results in an enhanced nutrient loading from continents via climatic warming. On the other hand, expanded shelves efficiently buffer the oceanic eutrophication.

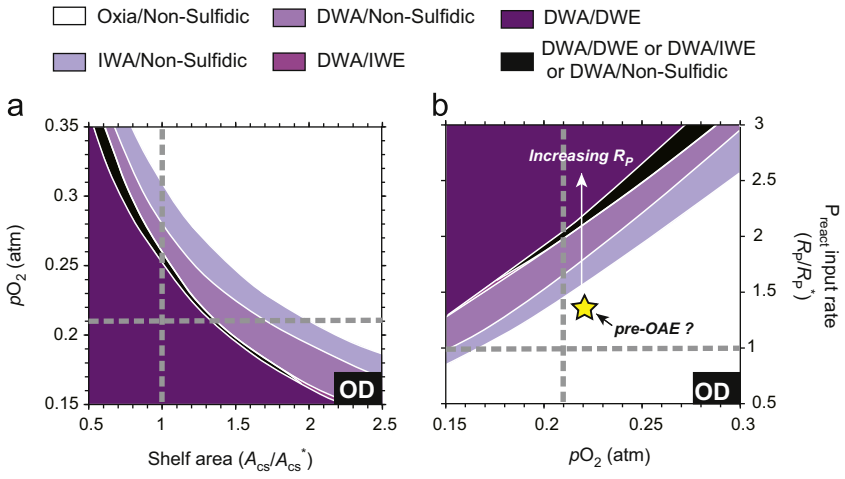

Fig. 6. Oceanic redox condition with respect to (a) atmospheric pO_2 and A_{cs}/A_{cs}^* ($R_P = 1.38 \times R_P^*$), and (b) R_P/R_P^* and pO_2 ($A_{cs} = 2.12 \times A_{cs}^*$) for the OD region under the Cretaceous condition. Abbreviations have the same meanings as in Fig. 4. The parameter region where bistable solutions (DWA/DWE or DWA/IEW or DWA/non-sulfidic) exist is colored by black shading.

Variations in the CO_2 degassing rate throughout Earth's history have played a key role in regulating the oceanic redox state.

4.3. Implications for the initiation of OAEs

Finally, we consider the causal mechanisms of Cretaceous OAEs. Previous studies have suggested that there is an intimate connection between the two most widespread Cretaceous OAEs (i.e., OAE 1a and OAE 2) and the activities of LIPs (e.g., Adams et al., 2010; Kuroda et al., 2007; Snow et al., 2005; Tejada et al., 2009; Turgeon and Creaser, 2008). Massive injections of greenhouse gases associated with the activity of LIPs may have caused a rapid climate warming and enhancement of chemical weathering on land. An enhanced nutrient loading to oceans would cause oceanic eutrophication and de-oxygenation. In fact, increases in phosphorus accumulation rate around the initial stage of OAEs have been reported for several geological sections (Bomou et al., 2013; Gertsch et al., 2010; Hetzel et al., 2011; Kraal et al., 2010; Mort et al., 2007a, 2007b, 2008; Nederbragt et al., 2004; Pearce et al., 2009; Scopelliti et al., 2010; Westermann et al., 2010), implying enhanced biological activity and/or enhanced phosphorus input from land. Isotopic variations of strontium, osmium and calcium also indicate the enhancement of continental weathering accompanied by OAEs (Blättler et al., 2011; Frijia and Parente, 2008; Tejada et al., 2009). Considering the high weatherability of basalt (Dessert et al., 2001), the emplacement of LIPs followed by chemical weathering could promote phosphorus input to the oceans. To assess R_P^{crit} with respect to OAEs under Cretaceous conditions, we conducted sensitivity experiment on the oceanic redox state in terms of R_P/R_P^* and pO_2 (Fig. 6b). In this calculation, we assumed $A_{cs}=2.12\times A_{cs}^*$ based on Walker et al. (2002).

Geologic records of the late Cenomanian show that ocean anoxia was already established in the proto-north Atlantic region before OAE2 (e.g., Monteiro et al., 2012). Therefore, the pre-Cretaceous ocean was likely located near (or in) the EoA. We can estimate such conditions at $pO_2=\sim 0.20$–0.22 atm (supposing $R_P=1.38\times R_P^*$). In such a case, a slight increase in R_P could cause widespread OAE. In contrast, if the Cretaceous pO_2 was high (>0.28 atm) (Bergman et al., 2004; Glasspool and Scott, 2010), then R_P^{crit} would be much higher ($>2.5\times R_P^*$), thus requiring a large climatic perturbation to cause an OAE. If a transient threefold increase in the continental weathering, as inferred from the calcium isotopic variation (Blättler et al., 2011), was the case, then widespread anoxia could have been triggered even if $pO_2=0.30$ atm. However, it is difficult to cause widespread euxinia, conflicting with the geological evidence (Monteiro et al., 2012). To cause pervasive euxinia by a threefold increase in R_P, Cretaceous atmospheric pO_2 should be lower than ~ 0.28 atm. Further investigations with a three-dimensional ocean model would make a logical next step towards assessing the relationship between paleoredox distribution, size of shelf area, and atmospheric pO_2 level, considering that paleogeography exerts an effect on the spatial distribution of anoxia/euxinia during the late Cretaceous (e.g., Meyer and Kump, 2008; Monteiro et al., 2012; Trabucho-Alexandre et al., 2010).

On the other hand, Handoh and Lenton (2003) claim that an increase in weathering forcing could drag the atmosphere–ocean system into a self-oscillating system, in which pO_2 has changes on the timescales of several millions of years. If so, high pO_2 conditions would be expected in the aftermath of an OAE and the pre-OAE pO_2 would be relatively low. Therefore, high pO_2 estimates (Bergman et al., 2004; Glasspool and Scott, 2010) and a series of OAEs during the Cretaceous may not be mutually inconsistent.

Although further investigation is required to test the linkages between the activities of LIPs, OAEs, and C–P–O biogeochemical dynamics, Fig. 6b demonstrates that an increase in R_P, which is promoted by a climatic warming caused by the activities of LIPs, could have caused Cretaceous OAEs.

5. Conclusions

We conducted a systematic sensitivity experiment with respect to the biogeochemical effects of the atmospheric pO_2 level, shelf area A_{cs}, and riverine P_{react} input rate R_P on the oceanic redox condition. Pervasive anoxia and euxinia will occur at $pO_2<0.145$ atm and $pO_2<0.125$ atm at the present values of A_{cs} and R_P. These critical values are higher than the previous estimate of $\sim$50% PAL, and reflect the preferential regeneration of P under anoxic waters. The sensitivity experiment for A_{cs} showed that changes in A_{cs} significantly affect marine redox by changing marine nutrient cycling. In particular, vast shelf areas result in oligotrophic and well-oxygenated conditions. We conclude that pO_2 and A_{cs} play a fundamental role in long-term oceanic redox.

We also assessed the oceanic redox state under Cretaceous "greenhouse" climatic conditions, highlighting the important role of A_{cs} on the marine redox state during the Cretaceous. If the vast A_{cs} ($\sim$200% of present) reconstructed from geomorphological studies (Ronov, 1994; Walker et al., 2002) is the case, an oxygenated oceanic condition would be achieved if $pO_2>\sim 0.21$ atm. Without considering this effect, the ocean becomes deoxygenated unless $pO_2>\sim 0.31$ atm. In other words, our results confirm that variations in sea-level stands (i.e., shelf size) are very likely to be a key controlling factor of the oceanic redox state on timescales longer than 10^6 yr. It is suggested that tectonic evolution, such as variations in the seafloor spreading rate and shelf area, and oceanic redox are much more intimately related with each other than previously thought.

We also found that an increase in R_P is an important mechanism for Cretaceous OAEs. However, the required perturbation is significantly affected by pO_2. Further investigation is needed to elucidate the connection between the activities of LIPs and OAEs as well as to better understand the biogeochemical dynamics during OAEs.

Acknowledgments

We are thankful to reviewers for constructive reviews and comments. This research was supported by the Sasakawa Scientific Research Grant from The Japan Science Society.

Appendix A. Formulation of the relationship between weathering rate and R_P

We discuss the relationship between the warm climatic conditions and ocean redox state in Section 4.2. To do this, we assumed several relationships between the climatic conditions and the weathering rate on land.

Phosphorus availability in the ocean is limited by the supply of P via chemical weathering of continents (apatite mineral is considered to be the primary phosphorus source; e.g., Föllmi, 1996; Guidry and Mackenzie, 2000). Since apatite is both in silicate and carbonate rocks, the discharge of P_{react} may be written as the sum of the two input rate coming from the weathering of silicate R_P^{sil} and carbonate rocks R_P^{carb}. Phosphorus is also derived from the oxidative weathering of old organic matter in sedimentary rock (i.e., kerogen). Hence, the total riverine P_{react} input rate R_P

may be written as

$$R_P = R_P^{sil} + R_P^{carb} + R_P^{org} \quad (A.1)$$

The contribution of each source is given by

$$R_P^{sil} = \alpha_{sil} W_{sil} \quad (A.2)$$

$$R_P^{carb} = W_{carb}/CP_{carb} \quad (A.3)$$

$$R_P^{org} = W_{org}/CP_{org} \quad (A.4)$$

where W_{sil}, W_{carb}, and W_{org} are weathering fluxes of silicate, carbonate, and organic matter, respectively. CP_{carb} and CP_{org} are molar ratios of carbon to phosphorus content in carbonate rock (=1000) and organic matter (=250), respectively. The factor α_{sil} is an adjustment parameter, which is determined such that R_P=0.18 T mol P/yr for reference condition. Although the factors controlling chemical weathering are complex, the rate of chemical weathering is usually considered to be temperature dependent (Berner, 2004; Dessert et al., 2001). Here we adopt a simple but well-calibrated formula from the GEOCARB model (e.g., Berner, 2004, 2006a, 2006b). Carbonate and silicate weathering is affected by soil biological activity due to land plants and bacteria, as well as many other factors. The complete weathering formula is given by

$$W_{carb} = f_{bio}(t) f_{Bc}(t) f_E(t) f_{AD}(t) f_{LA}(t) W^*_{carb} \quad (A.5)$$

$$W_{sil} = f_{volc}(t) f_{bio}(t) f_{Bt}(t) f_R(t) f_E(t) f_{AD}(t)^{0.65} W^*_{sil} \quad (A.6)$$

$$f_{AD} = f_A(t) f_D(t) \quad (A.7)$$

$$f_{LA} = f_L(t) f_A(t) \quad (A.8)$$

$$f_{bio} = \left(\frac{2 \cdot R_{CO_2}}{1 + R_{CO_2}} \right)^{0.4} \quad (A.9)$$

$$f_{Bt} = (1 + f_{sil} \Delta T)^{0.65} \exp(f_{zz} \Delta T) \quad (A.10)$$

$$f_{Bc} = (1 + f_{cal} \Delta T)^{0.65} \quad (A.11)$$

where t is the time in Myr, $R_{CO_2} = pCO_2/pCO_2^*$, pCO_2^*=280 ppm, an asterisk indicates the reference value, and ΔT is the deviation of the temperature from its reference value of 288.15 K. The meanings of $f(t)$ factors are according to GEOCARB model (e.g., Berner, 2004; 2006b). For the Cretaceous conditions, we assumed atmospheric pCO_2 levels of 1000 ppmv, which is in agreement with a recent reconstruction based on proxies (Hong and Lee, 2012; Park and Royer, 2011; Royer et al., 2012). All parameter values assumed in the calculation are listed in Table A1.

Table A1
Parameters for the calculation of weathering flux.

Parameter	Unit	Value
α_{sil}		56.2
W_{sil}^*	T mol(Ca+Mg)	6.8
W_{carb}^*	T mol(Ca+Mg)	12.9
W_{org}^*	T mol	11.5
f_E		0.8
f_R		0.705
f_{AD}		1.07
f_{LA}		0.94
f_{volc}		1.29
f_{sil}		0.038
f_{cal}		0.087
f_{ZZ}		0.09

We also assumed that the continental weathering of kerogen is affected by temperature and runoff.

$$W_{org} = f_{Bt}(t) f_R(t) f_{AD}(t) W^*_{org} \quad (A.12)$$

where W_{org}^* is the present weathering rate of organic matter.

The sedimentation rate (SR) at the seafloor is mainly affected by the input rate of terrigenous materials. We assumed a lowered SR to reflect the low physical erosion rate during the Cretaceous (Berner, 2006c; Berner and Kothavala, 2001):

$$SR(t,z) = 0.46 SR^*(z) \quad (A.13)$$

where z is the water depth in meters.

Appendix B. Supplementary material

Supplementary data associated with this article can be found in the online version at http://dx.doi.org/10.1016/j.epsl.2013.04.029.

References

Adams, D.D., Hurtgen, M.T., Sageman, B.B., 2010. Volcanic triggering of a biogeochemical cascade during Oceanic Anoxic Event 2. Nat. Geosci. 3, 201–204.

Algeo, T.J., Ingall, E., 2007. Sedimentary C_{org}:P ratios, paleocean ventilation, and Phanerozoic atmospheric pO_2. Palaeogeogr. Palaeoclimatol. Palaeoecol. 256, 130–155.

Ando, A., Kaiho, K., Kawahata, H., Kakegawa, T., 2008. Timing and magnitude of early Aptian extreme warming: unraveling primary $\delta^{18}O$ variation in indurated pelagic carbonates at Deep Sea Drilling Project Site 463, central Pacific Ocean. Palaeogeogr. Palaeoclimatol. Palaeoecol. 260, 463–476.

Armstrong, R.A., Lee, C., Hedges, J.I., Honjo, S., Wakeham, S.G., 2002. A new, mechanistic model for organic carbon fluxes in the ocean based on the quantitative association of POC with ballast minerals. Deep-Sea Res. II 49, 219–236.

Bergman, N.M., Lenton, T.M., Watson, A.J., 2004. COPSE: a new model of biogeochemical cycling over Phanerozoic time. Am. J. Sci. 304, 397–437.

Belcher, C.M., Yearsley, J.M., Hadden, R.M., McElwain, J.C., Rein, G., 2010. Baseline intrinsic flammability of Earth's ecosystems estimated from paleoatmospheric oxygen over the past 350 million years. Proc. Natl. Acad. Sci. 107, 22448–22453.

Berner, R.A., 1982. Burial of organic carbon and pyrite sulfur in the modern ocean: its geochemical and environmental significance. Am. J. Sci. 282, 451–473.

Berner, R.A., 1989. Biogeochemical cycles of carbon and sulfur and their effect on atmospheric oxygen over Phanerozoic time. Palaeogeogr. Palaeoclimatol. Palaeoecol. 75, 97–122.

Berner, R.A., 2004. The Phanerozoic Carbon Cycle: CO_2 and O_2. Oxford University Press, Oxford, p. 150.

Berner, R.A., 2006a. GEOCARBSULF: a combined model for Phanerozoic atmospheric O_2 and CO_2. Geochim. Cosmochim. Acta 70, 5653–5664.

Berner, R.A., 2006b. Inclusion of the weathering of volcanic rocks in the GEOCARBSULF model. Am. J. Sci. 306, 295–302.

Berner, R.A., 2006c. Comment: Mesozoic atmospheric oxygen. Am. J. Sci. 306, 769–771.

Berner, R.A., 2009. Phanerozoic atmospheric oxygen: new results using the GEOCARBSULF model. Am. J. Sci. 309, 603–609.

Berner, R.A., Kothavala, Z., 2001. GEOCARB III: a revised model of atmospheric CO_2 over Phanerozoic time. Am. J. Sci. 301, 182–204.

Betts, J.N., Holland, H.D., 1991. The oxygen content of ocean bottom waters, the burial efficiency of organic carbon, and the regulation of atmospheric oxygen. Palaeogeogr. Palaeoclimatol. Palaeoecol. 97, 5–18.

Bice, K.L., Norris, R.D., 2002. Possible atmospheric CO_2 extremes of the Middle Cretaceous (late Albian–Turonian). Paleoceanography 17, 1070, http://dx.doi.org/10.1029/2002PA000778.

Bjerrum, C.J., Bendtsen, J., Legarth, J.J.F., 2006. Modeling organic carbon burial during sea level rise with reference to the Cretaceous. Geochem. Geophys. Geosyst. 7, Q05008, http://dx.doi.org/10.1029/2005GC001032.

Blättler, C.L., Jenkyns, H.C., Reynard, L.M., Henderson, G.M., 2011. Significant increases in global weathering during Oceanic Anoxic Events 1a and 2 indicated by calcium isotopes. Earth Planet. Sci. Lett. 309, 77–88.

Bomou, B., Adatte, T., Tantawy, A.A., Mort, H., Fleitmann, D., Huang, Y., Föllmi, K.B., 2013. The expression of the Cenomanian–Turonian oceanic anoxic event in Tibet. Palaeogeogr. Palaeoclimatol. Palaeoecol. 369, 466–481.

Canfield, D.E., 1998. A new model for Proterozoic ocean chemistry. Nature 396, 450–453.

Canfield, D.E., Poulton, S.W., Knoll, A.H., Narbonne, G.M., Ross, G., Goldberg, T., Strauss, H., 2008. Ferruginous conditions dominated later Neoproterozoic deep-water chemistry. Science 321, 949–952.

Catling, D.C., Claire, M.W., 2005. How Earth's atmosphere evolved to an oxic state: a status report. Earth Planet. Sci. Lett. 237, 1–20.

Colman, A.S., Holland, H.D., 2000. The global diagenetic flux of phosphorus from marine sediments to the oceans; redox sensitivity and the control of atmospheric oxygen levels. In: Glenn, C.R., Prevot-Lucas, L., Lucus, J. (Eds.), Marine Authigenesis: From Global to Microbial. Special Publication 66. SEPM, pp. 21–33.

Dahl, T.W., Hammarlund, E.U., Anbar, A.D., Bond, D.P.G., Gill, B.C., Gordon, G.W., Knoll, A.H., Nielsen, A.T., Schovsbo, N.H., Canfield, D.E., 2010. Devonian rise in atmospheric oxygen correlated to the radiations of terrestrial plants and large predatory fish. Proc. Natl. Acad. Sci. 107, 17911–17915.

Dessert, C., Dupré, B., François, L.M., Schott, J., Gaillardet, J., Chakrapani, G., Bajpai, S., 2001. Erosion of Deccan Trap determined by river geochemistry: impact on the global climate and $^{87}Sr/^{86}Sr$ ratio of seawater. Earth Planet. Sci. Lett. 188, 459–474.

Dunne, J.P., Sarmiento, J.L., Gnanadesikan, A., 2007. A synthesis of global particle export from the surface ocean and cycling through the ocean interior and on the seafloor. Global Biogeochem. Cycles 21, GB4006, http://dx.doi.org/10.1029/2006GB002907.

Falkowski, P.G., Katz, M.E., Milligan, A.J., Fennel, K., Cramer, B.S., Aubry, M.P., Berner, R.A., Novacek, M.J., Zapol, W.M., 2005. The rise of oxygen over the past 205 million years and the evolution of large placental mammals. Science 309, 2202–2204.

Föllmi, K.B., 1996. The phosphorus cycle, phosphogenesis and marine phosphate-rich deposits. Earth Sci. Rev. 40, 55–124.

Forster, A., Schouten, S., Moriya, K., Wilson, P.A., Sinninghe Damsté, J.S., 2007. Tropical warming and intermittent cooling during the Cenomanian/Turonian oceanic anoxic event 2: sea surface temperature records from the equatorial Atlantic. Paleocanography 22, PA1219, http://dx.doi.org/10.1029/2006PA001349.

Frakes, L.A., Francis, J.E., Syktus, J.I., 1992. Climate Modes of the Phanerozoic. Cambridge University Press, Cambridge, 274 pp.

Friedrich, O., Norris, R.D., Erbacher, J., 2012. Evolution of middle to late Cretaceous oceans—A 55 m.y. record of Earth's temperature and carbon cycle. Geology 40, 107–110.

Frijia, G., Parente, M., 2008. Strontium isotope stratigraphy in the upper Cenomanian shallow-water carbonates of the southern Apennines: short-term perturbations of marine $^{87}Sr/^{86}Sr$ during the oceanic anoxic event 2. Palaeogeogr. Palaeoclimatol. Palaeoecol. 261, 15–29.

Garcia, H., Gordon, L.I., 1992. Oxygen solubility in seawater: better fitting equations. Limnol. Oceanogr. 37 (6), 1307–1312.

Gertsch, B., Keller, G., Adatte, T., Berner, Z., Kassab, A.S., Tantawy, A.A.A., El-Sabbagh, A.M., Stueben, D., 2010. Cenomanian–Turonian transition in a shallow water sequence of the Sinai, Egypt. Int. J. Sci. 99, 165–182.

Glasspool, I.J., Scott, A.C., 2010. Phanerozoic concentrations of atmospheric oxygen reconstructed from sedimentary charcoal. Nat. Geosci. 1, 627–630.

Guidry, M.W., Mackenzie, F.T., 2000. Apatite weathering and the Phanerozoic phosphorus cycle. Geology 28, 631–634.

Handoh, I.C., Lenton, T.M., 2003. Periodic mid-Cretaceous oceanic anoxic events linked by oscillations of the phosphorus and oxygen biogeochemical cycles. Global Biogeochem. Cycles 17 (4), http://dx.doi.org/10.1029/2003GB002039.

Hedges, J.I., Keil, R.G., 1995. Sedimentary organic matter preservation: an assessment and speculative synthesis. Mar. Chem. 49, 81–115.

Henrichs, S.M., Reeburgh, W.S., 1987. Anaerobic mineralization of marine sediment organic matter: rates and the role of anaerobic processes in the oceanic carbon economy. Geomicrobiol. J. 5, 191–237.

Hetzel, A., März, C., Vogt, C., Brumsack, H.-J., 2011. Geochemical environment of Cenomanian–Turonian black shale deposition at Wunstorf (northern Germany). Cretaceous Res. 32, 480–494.

Hong, S.K., Lee, Y.I., 2012. Evaluation of atmospheric carbon dioxide concentrations during the Cretaceous. Earth Planet. Sci. Lett. 327–328, 23–28.

Hotinski, R.M., Kump, L.R., Najjar, R.G., 2000. Opening Pandra's Box: the impact of open system modeling on interpretations of anoxia. Paleoceanography 15, 267–279.

Hotinski, R.M., Bice, K.L., Kump, L.R., Najjar, R.G., Arthur, M.A., 2001. Ocean stagnation and end-Permian anoxia. Geology 29, 7–10.

Ingall, E.D., Jahnke, R., 1994. Evidence for enhanced phosphorus regeneration from marine sediments overlain by oxygen depleted waters. Geochim. Cosmochim. Acta 58, 2571–2575.

Ittekkot, V., 1993. The abiotically driven biological pump in the ocean and short-term fluctuations in atmospheric CO_2 contents. Global Planet. Change 8, 17–25.

Jenkyns, H.C., 2010. Geochemistry of oceanic anoxic events. Geochem. Geophys. Geosyst. 11, Q03004, http://dx.doi.org/10.1029/2009GC002788.

Joos, F., Sarmiento, J.L., Siegenthaler, U., 1991. Estimates of the effect of Southern Ocean iron fertilization on atmospheric CO_2 concentration. Nature 349, 772–775.

Kashiyama, Y., Ozaki, K., Tajika, E., 2011. Impact of the evolution of carbonate ballasts on marine biogeochemistry in the Mesozoic and associated changes in energy delivery to subsurface waters. Paleontol. Res. 15, 89–99.

Klaas, C., Archer, D.E., 2002. Association of sinking organic matter with various types of mineral ballast in the deep sea: implications for the rain ratio. Global Biogeochem. Cycles 16 (4), 1116, http://dx.doi.org/10.1029/2001GB001765.

Kraal, P., Slomp, C.P., Forster, A., Kuypers, M.M.M., 2010. Phosphorus cycling from the margin to abyssal depths in the proto-Atlantic during oceanic anoxic event 2. Palaeogeogr. Palaeoclimatol. Palaeoecol. 295, 42–54.

Kuroda, J., Ogawa, N.O., Tanimizu, M., Coffin, M.F., Tokuyama, H., Kitazato, H., Ohkouchi, N., 2007. Contemporaneous massive subaerial volcanism and late Cretaceous Oceanic Anoxic Event 2. Earth Planet. Sci. Lett. 256, 211–223.

Kuypers, M.M.M., Pancost, R.D., Nijenhuis, I.A., Sinninghe Damsté, J.S., 2002. Enhanced productivity let to increased organic carbon burial in the euxinic North Atlantic basin during the late Cenomanian oceanic anoxic event. Paleoceanography 17, 1051, http://dx.doi.org/10.1029/2000PA000569.

Larson, R.L., 1991. Geological consequences of superplumes. Geology 19, 963–966.

Lasaga, A.C., 1989. A new approach to isotopic modeling of the variation of atmospheric oxygen through the Phanerozoic. Am. J. Sci. 289, 411–435.

Lasaga, A.C., Ohmoto, H., 2002. The oxygen geochemical cycle: dynamics and stability. Geochim. Cosmochim. Acta 66, 361–381.

Leckie, R.M., Bralower, T.J., Cashman, R., 2002. Oceanic anoxic events and plankton evolution: biotic response to tectonic forcing during the mid-Cretaceous. Paleoceanography 17, http://dx.doi.org/10.1029/2001PA000623.

Lenton, T.M., 2003. The coupled evolution of life and atmospheric oxygen. In: Rothschild, L., Lister, A. (Eds.), Evolution on Planet Earth: The Impact of the Physical Environment. Academic Press, London, pp. 35–53.

Li, C., Love, G.D., Lyons, T.W., Fike, D.A., Sessions, A.L., Chu, X., 2010. A stratified redox model for the Ediacaran ocean. Science 328, 80–83.

Logan, G.A., Hayes, J.M., Hieshima, G.B., Summons, R.E., 1995. Terminal Proterozoic reorganization of biogeochemical cycles. Nature 376, 53–56.

Meyer, K.M., Kump, L.R., 2008. Oceanic euxinia in Earth history: causes and consequences. Annu. Rev. Earth Planet. Sci. 36, 251–288.

Meyer, K.M., Kump, L.R., Ridgwell, A., 2008. Biogeochemical controls on photic-zone euxinia during the end-Permian mass extinction. Geology 36, 747–750.

Miller, K., Kominz, M.A., Browning, J.V., Wright, J.D., Mountain, G.S., Katz, M.E., Sugarman, P.J., Cramer, B.S., Christie-Blick, N., Pekar, S.F., 2005. The Phanerozoic record of global sea-level change. Science 310, 1293–1298.

Monteiro, F.M., Pancost, R.D., Ridgwell, A., Donnadieu, Y., 2012. Nutrients as the dominant control on the spread of anoxia and euxinia across the Cenomanian–Turonian oceanic anoxic event (OAE2): model-data comparison. Paleoceanography 27, PA4209, http://dx.doi.org/10.1029/2012PA002351.

Mort, H.P., Adatte, T., Föllmi, K.B., Keller, G., Steinmann, P., Matera, V., Berner, Z., Stüben, D., 2007a. Phosphorus and the roles of productivity and nutrient recycling during oceanic anoxic event 2. Geology 35, 483–486.

Mort, H., Jacquat, O., Adatte, T., Steinmann, P., Föllmi, K., Matera, V., Berner, Z., Stüben, D., 2007b. The Cenomanian/Turonian anoxic event at the Bonarelli Level in Italy and Spain: enhanced productivity and/or better preservation? Cretaceous Res. 28, 597–612.

Mort, H.P., Adatte, T., Keller, G., Bartels, D., Föllmi, K.B., Steinmann, P., Berner, Z., Chellai, E.H., 2008. Organic carbon deposition and phosphorus accumulating during Oceanic Anoxic Event 2 in Tarfaya, Morocco. Cretaceous Res. 29, 1008–1023.

Müller, R.D., Sdrolias, M., Gaina, C., Steinberger, B., Heine, C., 2008. Long-term sea-level fluctuations driven by ocean basin dynamics. Science 319, 1357–1362.

Nederbragt, A.J., Thurow, J., Vonhof, H., Brumsack, H.-J., 2004. Modelling oceanic carbon and phosphorus fluxes: implications for the cause of the late Cenomanian Oceanic Anoxic Event (OAE2). J. Geol. Soc. London 161, 721–728.

Ozaki, K., Tajima, S., Tajika, E., 2011. Conditions required for oceanic anoxia/euxinia: constraints from a one-dimensional ocean biogeochemical cycle model. Earth Planet. Sci. Lett. 304, 270–279.

Park, J., Royer, D.L., 2011. Geologic constraints on the glacial amplification of Phanerozoic climate sensitivity. Am. J. Sci. 311, 1–26.

Pearce, M.A., Jarvis, I., Tocher, B.A., 2009. The Cenomanian-Turonian boundary event, OAE2 and palaeoenvironmental change in epicontinental seas: new insights from the dinocyst and geochemical records. Palaeogeogr. Palaeoclimatol. Palaeoecol. 280, 207–234.

Planavsky, N.J., McGoldrick, P., Scott, C.T., Li, C., Reinhard, C.T., Kelly, A.E., Chu, X., Bekker, A., Love, G.D., Lyons, T.W., 2011. Widespread iron-rich conditions in the mid-Proterozoic ocean. Nature 477, 448–451.

Poulton, S.W., Fralick, P.W., Canfield, D.E., 2010. Spatial variability in oceanic redox structure 1.8 billion years ago. Nat. Geosci. 3, 486–490.

Pucéat, E., Lécuyer, C., Sheppard, S.M.F., Dromart, G., Reboulet, S., Grandjean, P., 2003. Thermal evolution of Cretaceous Tethyan marine waters inferred from oxygen isotope composition of fish tooth enamels. Paleoceanography 18, 1029, http://dx.doi.org/10.1029/2002PA000823.

Ronov, A.B., 1968. Probable changes in the composition of sea water during the course of geologic time. Sedimentology 10, 25–43.

Ronov, A.B., 1994. Phanerozoic transgressions and regressions on the continents: a quantitative approach based on areas flooded by the sea and areas of marine and continental deposition. Am. J. Sci. 294, 777–801.

Royer, D.L., Berner, R.A., Montanez, I.P., Tabor, N.J., Beerling, D.J., 2004. CO_2 as a primary driver of Phanerozoic climate. GSA Today 14, http://dx.doi.org/10.1130/1052-5173.

Royer, D.L., Pagani, M., Beerling, D.J., 2012. Geobiological constraints on Earth system sensitivity to CO_2 during the Cretaceous and Cenozoic. Geobiology, http://dx.doi.org/10.1111/j.1472-4669.2012.00320.x.

Sageman, B.B., Meyers, S.R., Arthur, M.A., 2006. Orbital time scale and new C-isotope record for Cenomanian–Turonian boundary stratotype. Geology 34, 125–128.

Sarmiento, J.L., Herbert, T.D., Toggweiler, J.R., 1988. Causes of anoxia in the world ocean. Global Biogeochem. Cycles 2 (2), 115–128.

Scopelliti, G., Bellanca, A., Neri, R., Sabatino, N., 2010. Phosphogenesis in the Bonarelli Level from northwestern Sicily, Italy: petrographic evidence of microbial mediation and related REE behaviour. Cretaceous Res. 31, 237–248.

Scott, C., Lyons, T.W., Bekker, A., Shen, Y., Poulton, W., Chu, X., Anbar, A.D., 2008. Tracing the stepwise oxygenation of the Proterozoic ocean. Nature 452, 456–460.

Shaffer, G., 1989. A model of biogeochemical cycling of phosphorus, nitrogen, oxygen, and sulfur in the ocean: one step toward a global climate model. J. Geophys. Res. 94, 1979–2004.
Shaffer, G., 1996. Biogeochemical cycling in the global ocean 2. New production, Redfield ratios, and remineralization in the organic pump. J. Geophys. Res. 101, 3723–3745.
Shaffer, G., Sarmiento, J.L., 1995. Biogeochemical cycling in the global ocean 1. A new, analytical model with continuous vertical resolution and high-latitude dynamics. J. Geophys. Res. 100, 2659–2672.
Shen, Y., Canfield, D.E., Knoll, A.H., 2002. Middle Proterozoic ocean chemistry: evidence from the McArthur Basin, Northern Australia. Am. J. Sci. 302, 81–109.
Shen, Y., Knoll, A.H., Walter, M.R., 2003. Evidence for low sulphate and anoxia in mid-Proterozoic marine basin. Nature 423, 632–635.
Siegenthaler, U., Joos, F., 1992. Use of a simple model for studying oceanic tracer distributions and the global carbon cycle. Tellus 44B, 186–207.
Slomp, C.P., Van Cappellen, P., 2007. The global marine phosphorus cycle: sensitivity to oceanic circulation. Biogeosciences 4, 155–171.
Snow, L.J., Duncan, R.A., Bralower, T.J., 2005. Trace element abundances in the Rock Canyonn Anticline, Pueblo, Colorado, marine sedimentary section and their relationship to Caribbean plateau construction and oxygen anoxic event 2. Paleoceanography 20, PA3005, http://dx.doi.org/10.1029/2004PA001093.
Southam, J.R., Peterson, W.H., Brass, G.W., 1982. Dynamics of anoxia. Palaeogeogr. Palaeoclimatol. Palaeoecol. 40, 183–198.
Southam, J.R., Peterson, W.H., Brass, G.W., 1987. A model of global and basin-scale anoxia. Math. Model. 9, 125–145.
Strauss, H., 2006. Anoxia through time. In: Neretin, L.N. (Ed.), Past and Present Water Column Anoxia. NATO Science Series. IV. Earth and Environmental Sciences. Springer, Netherlands, pp. 3–19.
Tejada, M.L.G., Suzuki, K., Kuroda, J., Coccioni, R., Mahoney, J.J., Ohkouchi, N., Sakamoto, T., Tatsumi, Y., 2009. Ontong Java Plateau eruption as a trigger for the early Aptian oceanic anoxic event. Geology 37, 855–858.
Trabucho-Alexandre, J., Tuenter, E., Henstra, G.A., van der Zwan, K.J., van de Wal, R.S.W., Dijkstra, H.A., de Boer, P.L., 2010. The mid-Cretaceous North Atlantic nutrient trap: black shales and OAEs. Paleocanography 25, PA4201, http://dx.doi.org/10.1029/2010PA001925.
Tsandev, I., Slomp, C.P., 2009. Modeling phosphorus cycling and carbon burial during Cretaceous Oceanic Anoxic Events. Earth Planet. Sci. Lett. 286, 71–79.
Turgeon, S.C., Creaser, R.A., 2008. Cretaceous oceanic anoxic event 2 triggered by a massive magmatic episode. Nature 454, 323–327.
Van Cappellen, P., Ingall, E., 1996. Redox stabilization of the atmosphere and oceans by phosphorus-limited marine productivity. Science 271, 493–496.
Voigt, S., Erbacher, J., Mutterlose, J., Weiss, W., Westerhold, T., Wiese, F., Wilmsen, M., Wonik, T., 2008. The Cenomanian–Turonian of the Wunstorf section—(North Germany): global stratigraphic reference section and new orbital time scale for Oceanic Anoxic Event 2. Newsl. Stratigr. 43, 65–89.
Walker, J.C.G., 1974. Stability of atmospheric oxygen. Am. J. Sci. 274, 193–214.
Walker, L.J., Wilkinson, B.H., Ivany, L., 2002. Continental drift and Phanerozoic Carbonate Accumulation in shallow-shelf and deep-marine settings. J. Geol. 110, 75–87.
Wallmann, K., 2003. Feedbacks between oceanic redox states and marine productivity: a model perspective focused on benthic phosphorus cycling. Global Biogeochem. Cycles 17, 1084, http://dx.doi.org/10.1029/2002GB00968.
Westermann, S., Caron, M., Fiet, N., Fleimann, D., Matera, V., Adatte, T., Föllmi, K.B., 2010. Evidence for oxic conditions during oceanic anoxic event 2 in the northern Tethyan pelagic realm. Cretaceous Res. 31, 500–514.
Winguth, C., Winguth, A.M.E., 2012. Simulating Permian-Triassic oceanic anoxia distribution: implication for species extinction and recovery. Geology 40, 127–130.